Dinuclear Tb and Dy Complexes supported by hybrid Schiff-Base/Calixarene Ligands: Synthesis, Structures and Magnetic Properties

Peter Hahn,[a] Steve Ullmann,[a] Jennifer Klose,[a] Yan Peng,[b] Annie K. Powell,[b] Berthold Kersting[a]

[a] *Institut für Anorganische Chemie, Universität Leipzig, Johannisallee 29, D-04103 Leipzig, Germany. E-mail: b.kersting@uni-leipzig.de; Fax: +49/(0)341-97-36199*

[b] *Institute of Inorganic Chemistry, Karlsruhe Institute of Technology, Engesserstrasse 15, D-76131 Karlsruhe, Germany. E-mail: annie.powell@kit.edu*

Supporting Information

Contents

1. Characterization of compounds

a) NMR spectroscopy (for H_3L^2)

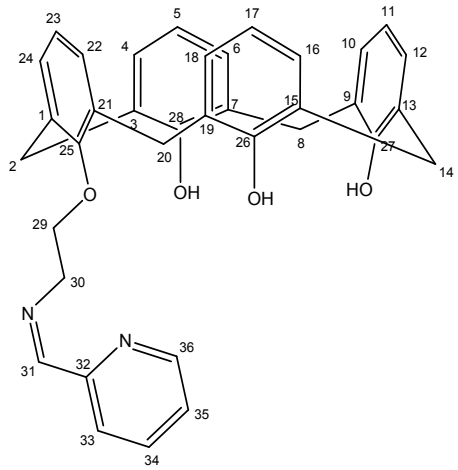

Figure S1. Labeling scheme of H_3L^2 used for assignment of ^1H and ^{13}C NMR signals.

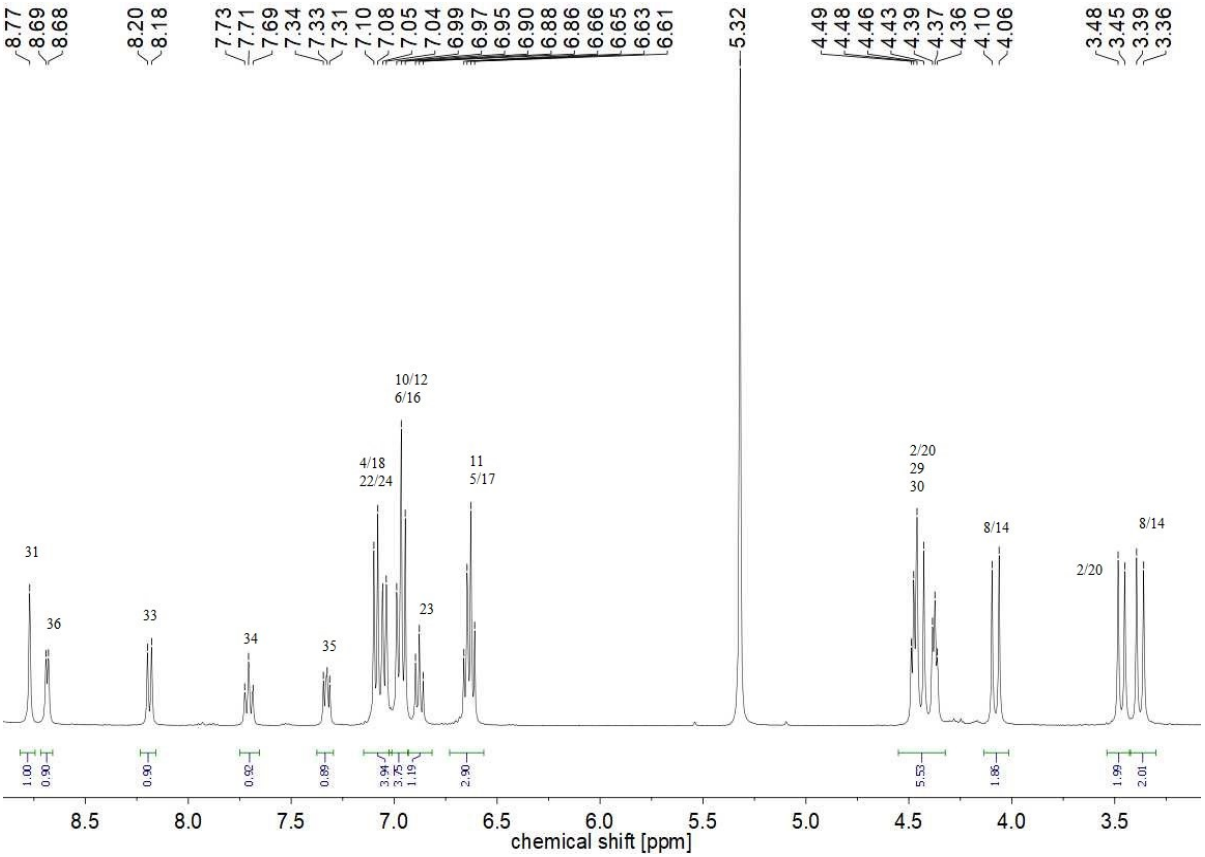

Figure S2. ^1H NMR spectrum of H_3L^2 in CD_2Cl_2 at ambient temperature.

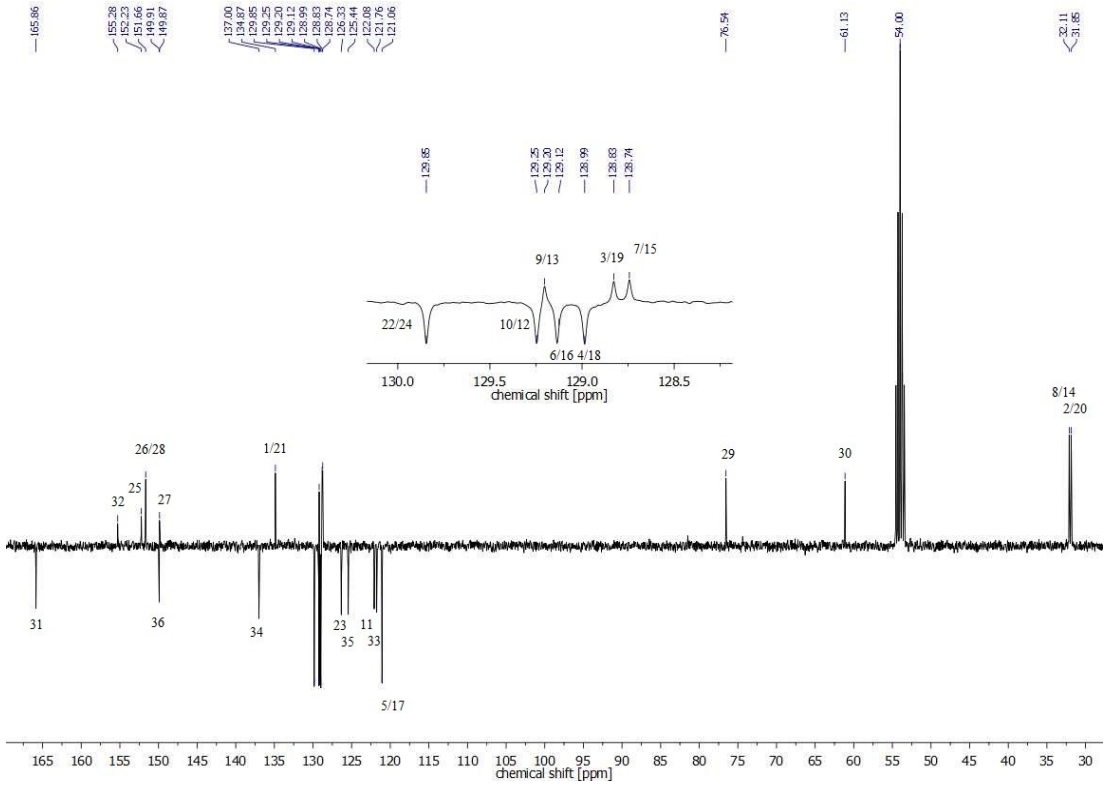

Figure S3. APT NMR spectrum of H_3L^2 in CD_2Cl_2 at ambient temperature. The inset shows the spectral range between 128 ppm and 130 ppm.

b) ESI-MS-spectrometry

Ligand H_3L^2

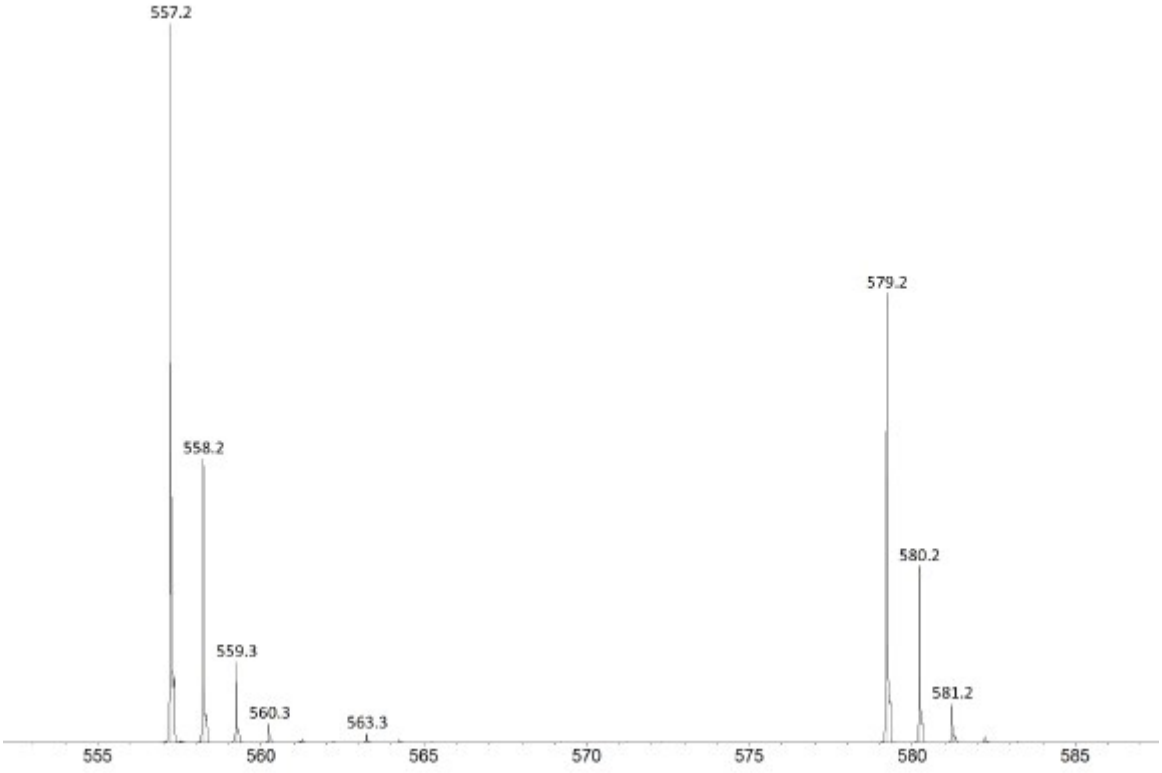

Figure S4. ESI(+)-MS of H_3L^2 in MeCN in the *m*/z range 555-585.

Complex $[HNEt_3][Dy_2(HL^1)(L^1)]$ (**5**).

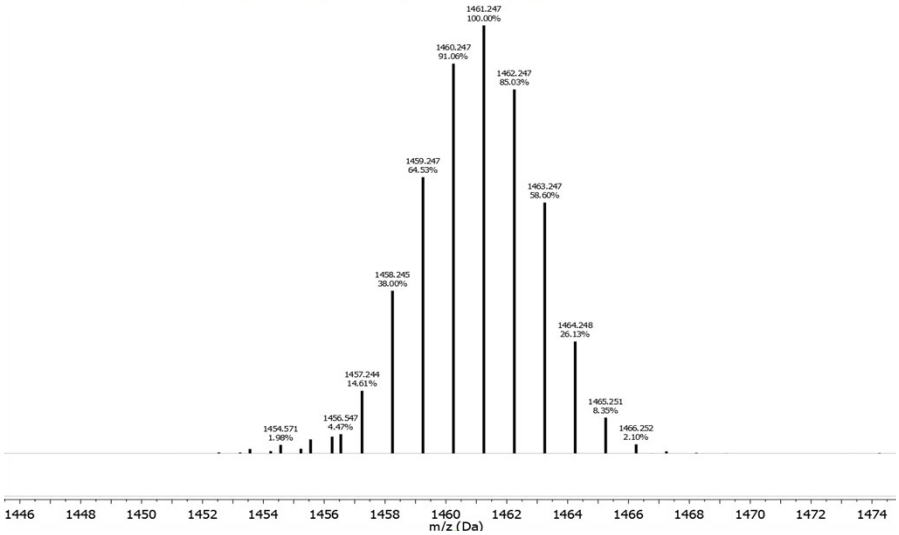

Figure S5. ESI(-)-MS of $[HNEt_3][Dy_2(HL^1)(L^1)]$ (**5**) in MeCN in the *m*/z range 1446-1474.

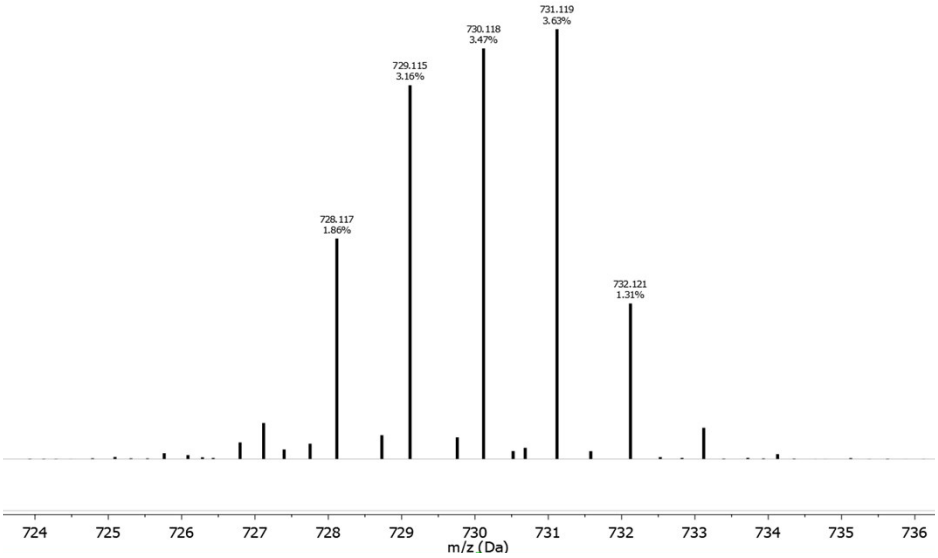

Figure S6. ESI(-)-MS of $[HNEt_3][Dy_2(HL^1)(L^1)]$ (**5**) in MeCN (*m*/*z* 724-736).

Complex $[Tb_2(L^2)_2]\cdot 4MeCN$ (**7**).

Figure S7. ESI(+)-MS of $[Tb_2(L^2)_2]\cdot 4MeCN$ (**7**) in MeCN (*m*/*z* 1447-1468).

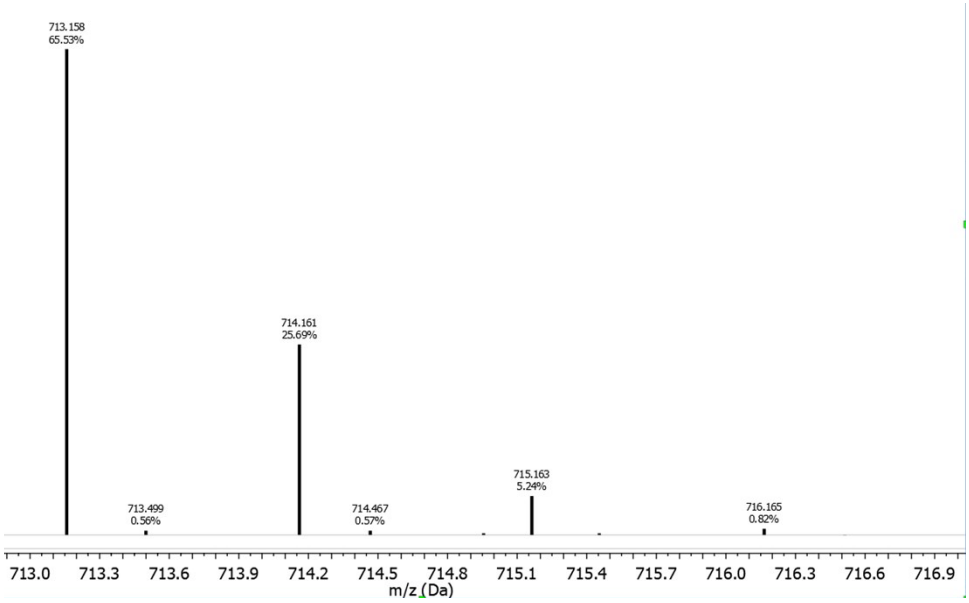

Figure S8. ESI(+)-MS of $[Tb_2(L^2)_2]\cdot 4MeCN$ (**7**) in MeCN (*m*/*z* 713-717).

Complex $[Dy_2(L^2)_2]\cdot 4MeCN$ (**8**).

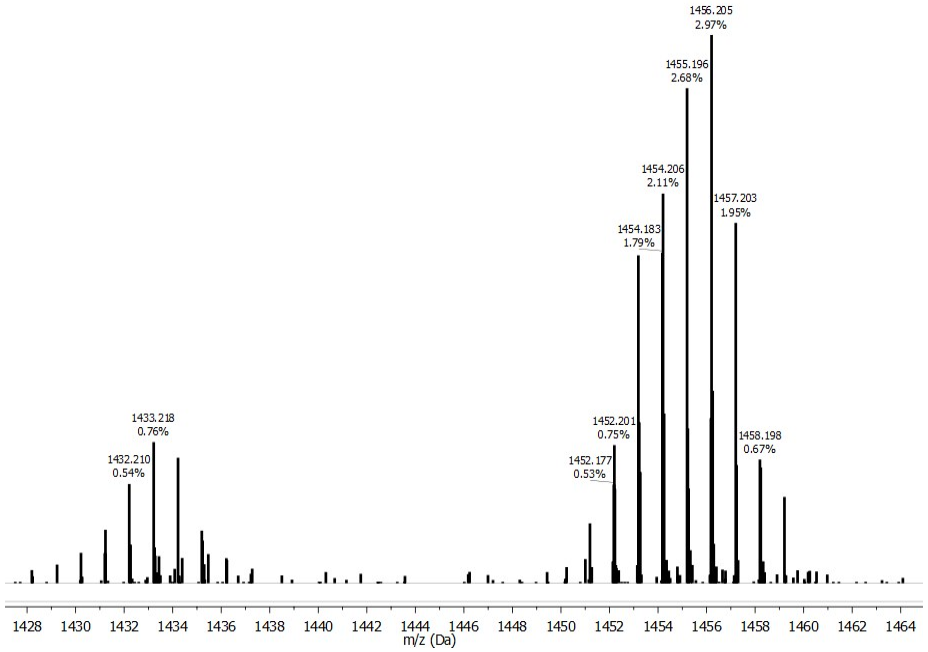

Figure S9. ESI(+)-MS of $[Dy_2(L^2)_2]\cdot 4MeCN$ (**8**) in MeCN (*m*/*z* 1428-1464).

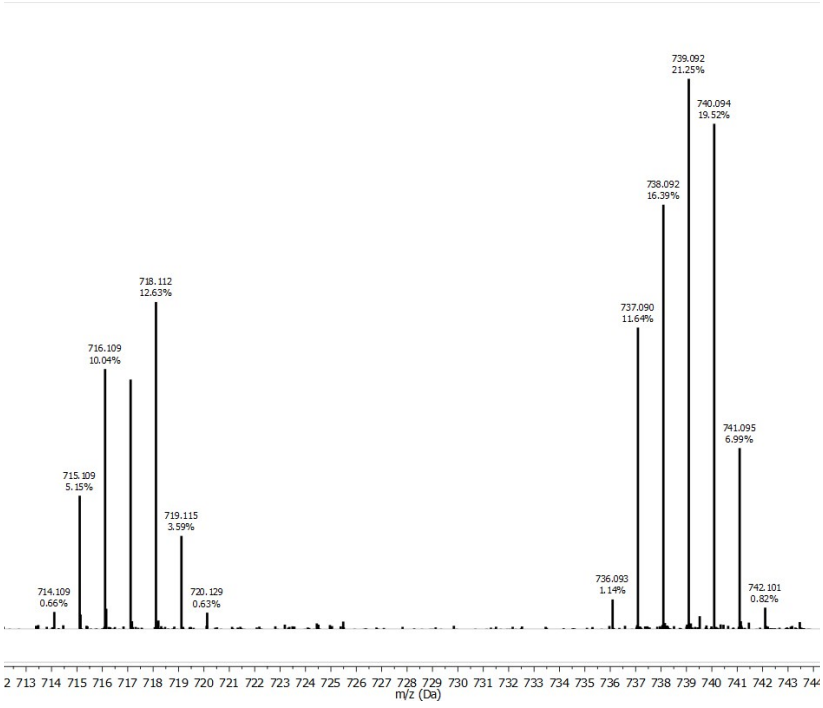

Figure S10. ESI(+)-MS of $[Dy_2(L^2)_2]\cdot 4MeCN$ (**8**) in MeCN (*m*/*z* 713-743).

c) FT-IR spectra

Complex $[HNEt_3][Dy_2(HL^1)(L^1)]$ (**5**).

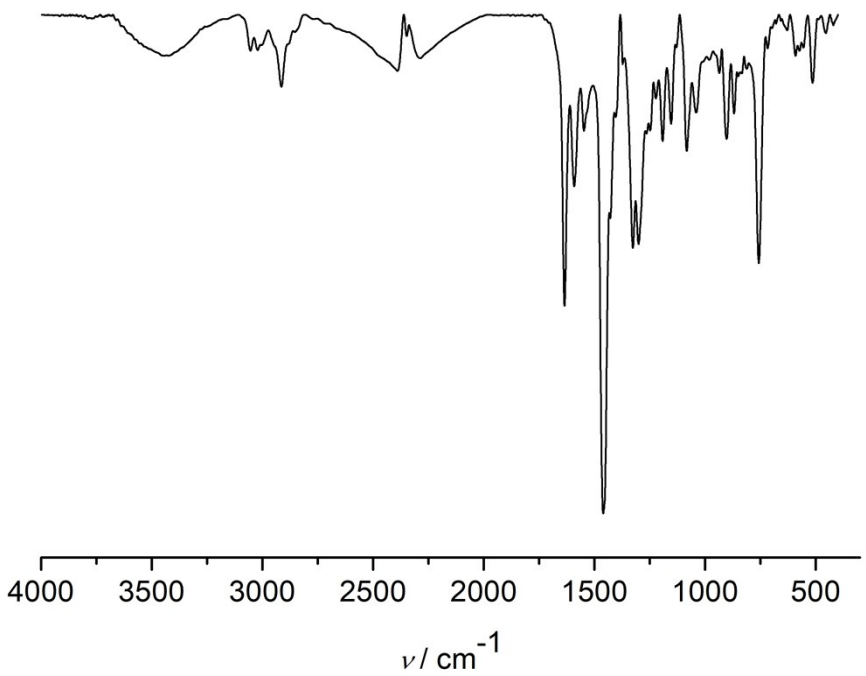

Figure S11. FT-IR spectrum of $[HNEt_3][Dy_2(HL^1)(L)]$ (**5**).

Ligand H_3L^2, Complexes $[Tb_2(L^2)_2]\cdot 4MeCN$ (**7**) and $[Dy_2(L^2)_2]\cdot 4MeCN$ (**8**).

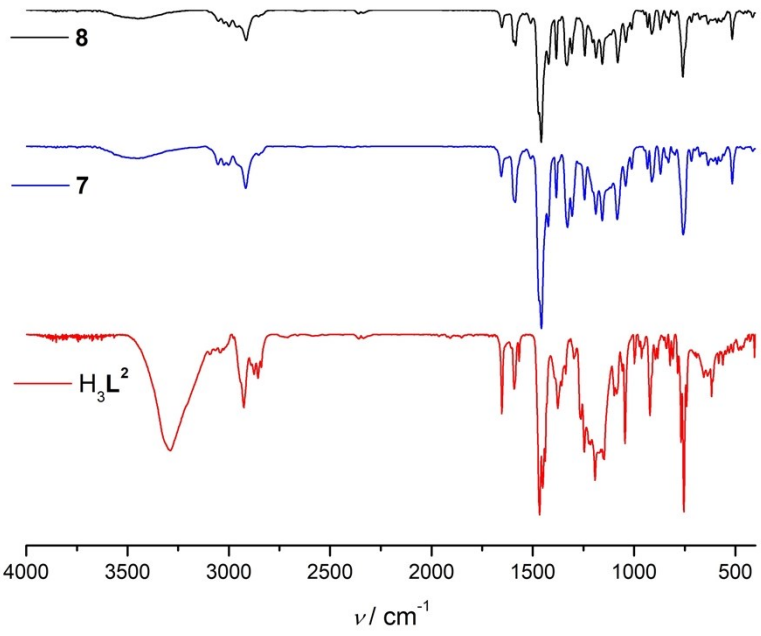

Figure S12. FT-IR spectra of H_3L^2, $[Tb_2(L^2)_2]\cdot 4MeCN$ (**7**) and $[Dy_2(L^2)_2]\cdot 4MeCN$ (**8**).

2. X-ray crystallography

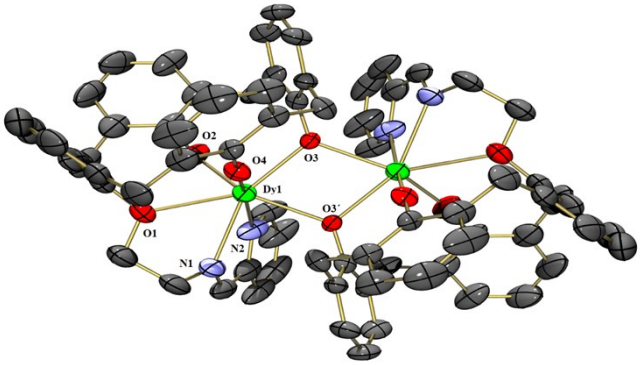

Figure S13. ORTEP representation of the molecular structure of the neutral Dy_2 complex in crystals of $[Dy_2(L^2)_2]$·4MeCN (**8**·4MeCN). Thermal ellipsoids are shown at the 30% probability level. MeCN molecules omitted for clarity.

Coordination Geometries

Determination of coordination geometries of the lanthanide ion in complexes **3**, **7**, and **8** utilizing SHAPE[1]: According to SHAPE, deviations from ideal coordination geometry are represented by a factor, that increases upon increasing distortions from the ideal geometry, for which the deviation factor is zero.

Compound $(HNEt_3)[Gd_2(HL^1)(L^1)]$ (**3**)[2]

Gd1:
Pentagonal bipyramid: Gd1: 4.519,
Capped octahedron: Gd1: 2.257
Capped trigonal prism: Gd1: 2.616
Johnson pentagonal bipyramid: 7.260

Gd2:
Pentagonal bipyramid: 4.050
Capped octahedron: 2.368
Capped trigonal prism: 2.369
Johnson pentagonal bipyramid: 6.941

According to SHAPE, the coordination geometry of the seven-coordinate Gd1 atom is intermediate between capped octahedral or capped trigonal prismatic. The same applies to the

seven-coordinate Gd2 ion (2.368). Complex **5** is assumed to be isostructural to complex **3** and to exhibit similar coordination environments.

Compound $[Tb_2(L^2)_2]\cdot 4MeCN$ (7·4MeCN):

Several coordination environments were considered for the seven-coordinate Tb^{III} ions in **7**. Of these, the capped octahedral environment appears to show the smallest deviation from the ideal value. However, the differences to the capped trigonal prismatic environment are not very pronounced:

Pentagonal bipyramid: 6.647

Capped octahedron: 4.191

Capped trigonal prism: 4.535

Johnson pentagonal bipyramid: 10.593

Compound $[Dy_2(L^2)_2]\cdot 4MeCN$ (8·4MeCN):

Several coordination environments were considered for the seven-coordinate Dy^{III} ions in **8**. Of these, the capped octahedral or trigonal prismatic environment appear to show the smallest deviation from the ideal values. However, as above, the differences are not very pronounced:

Pentagonal bipyramid: 6.241

Capped octahedron: 4.169

Capped trigonal prism: 4.429

Johnson pentagonal bipyramid: 10.325

3. Squid Magnetometry

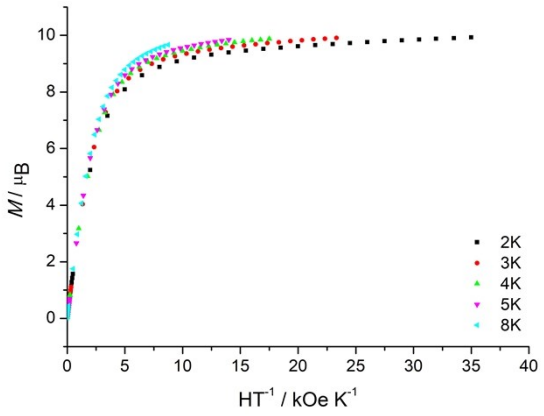

Figure S14. Plot of *M* versus *H/T* for $[HNEt_3][Dy_2(HL^1)(L^1)]$ (**5**) at temperatures at or below 8 K.

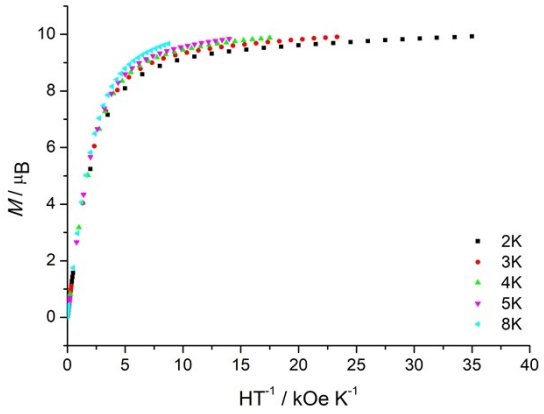

Figure S15. Plot of *M* versus *H/T* for $[Tb_2(L^2)_2]$ (**7**) at temperatures at or below 8 K.

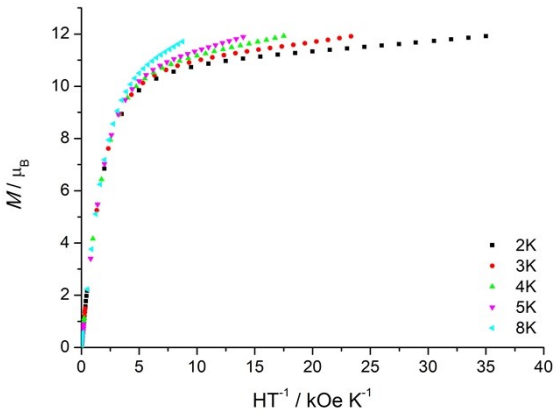

Figure S16. Plot of *M* versus *H/T* for $[Dy_2(L^2)_2]$ (**8**) at temperatures at or below 8 K.

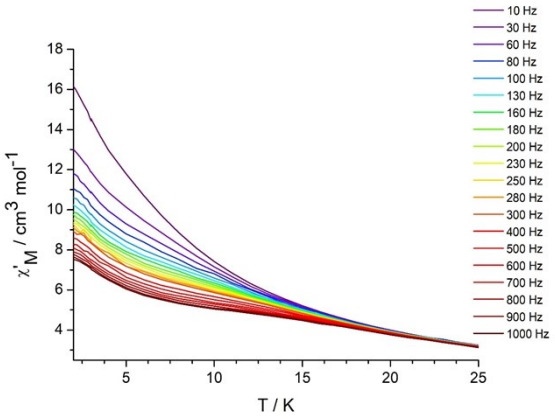

Figure S17. Frequency dependence of the in-phase (χ′) ac susceptibility from 2 to 25 K under an applied static field (3000 Oe) at indicated frequencies for the Dy^{III}_2 complex **5**.

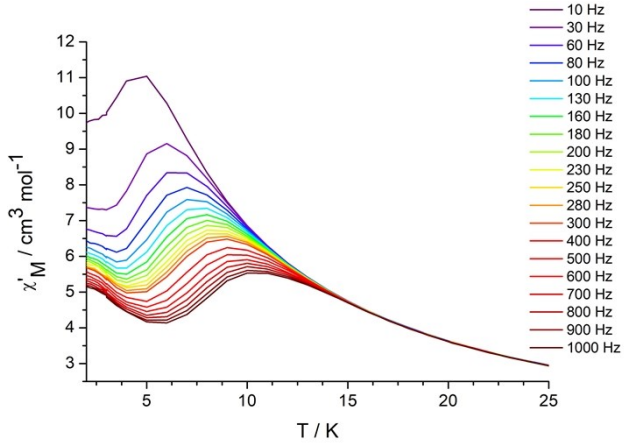

Figure S18. Frequency dependence of the in-phase (χ′) ac susceptibility from 2 to 25 K under an applied static field (3000 Oe) at indicated frequencies for the Dy^{III}_2 complex **8**.

Analysis of the AC susceptibility data.

The AC susceptibility data $\chi_{AC}(\omega)$ for **5** and **8** were analyzed utilizing the program CC-FIT2,[3] which fits the in-phase and out-of phase susceptibility data simultaneously using the Cole-Cole expression eq. 1,[4] where χ_S represents the adiabatic susceptibility, χ_S is the isothermal susceptibility, ω is defined as 2πν, τ is the magnetic relaxation time, and α is the Cole-Cole parameter ($0 < \alpha < 1$) quantifying the width of the τ distribution.

$$\chi_{AC}(\omega) = \chi_S + (\chi_T - \chi_S)/((1+(i\omega\tau)(1-\alpha)) \quad (1)$$

The experimental $\chi_{AC}(\omega)$ curves for **5** were fitted applying eq 1 and are plotted as the

$\chi'(\omega)$,$\chi''(\omega)$ and Cole-Cole plots in Fig. S19. Table S1 lists the parameters obtained. As can be seen, the Cole-Cole plots reveal a distorted semi-circular form. Also the Cole-Cole parameter varies from 0.40 to 0.53 within the temperature range from 5 – 14 K indicating a wider distribution of relaxation time or more than one relaxation process in **5**. Unfortunately, analysis of the Cole-Cole plot at low temperature is not accessible with our setup. Thus, only the high-temperature regime of the Cole-Cole could be fitted. A plot of the corresponding relaxation times versus reciprocal temperature, reveals an Arrhenius–like behaviour (eq. 2, Fig. S20), with an effective energy barrier U_{eff} of 18.21 cm^{-1} (26.2 K) and a pre-exponential factor ($\tau_0 = 3.11 \cdot 10^{-5}$ s).

$$\tau = \tau_0 \exp(U_{eff}/kT) \qquad (2)$$

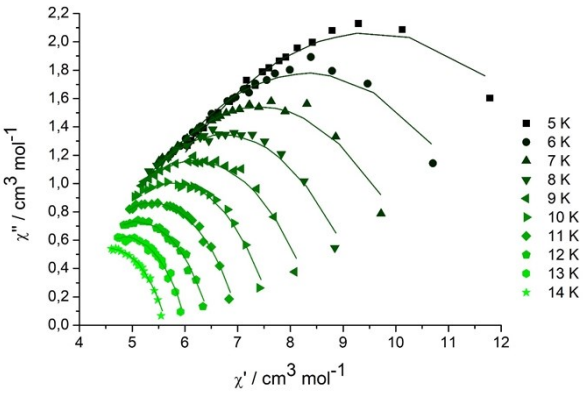

Figure S19. Cole-Cole plot for the Dy^{III}_2-compound **5** (for 3 kOe).

Table S1. Parameters resultant from fitting AC data of complex **5** (for 3 kOe).

T (K)	χ_S (cm^3/mol)	χ_T (cm^3/mol)	T	α	Residual
5	4.25445	14.8098	0.00301	0.5260	0.10594
6	4.12336	12.5088	0.00188	0.4894	0.09491
7	4.00687	10.8243	0.00122	0.4599	0.06436
8	3.89747	9.54153	0.00083	0.4347	0.04238
9	3.80368	8.57150	0.00061	0.4242	0.03903
10	3.81234	7.71339	0.00045	0.3935	0.01957
11	3.71898	7.05402	0.00033	0.3926	0.01205
12	3.70361	6.48964	0.00026	0.3874	0.01053
13	3.71413	6.02764	0.00022	0.3756	0.01068
14	3.53645	5.64504	0.00016	0.3994	0.00700

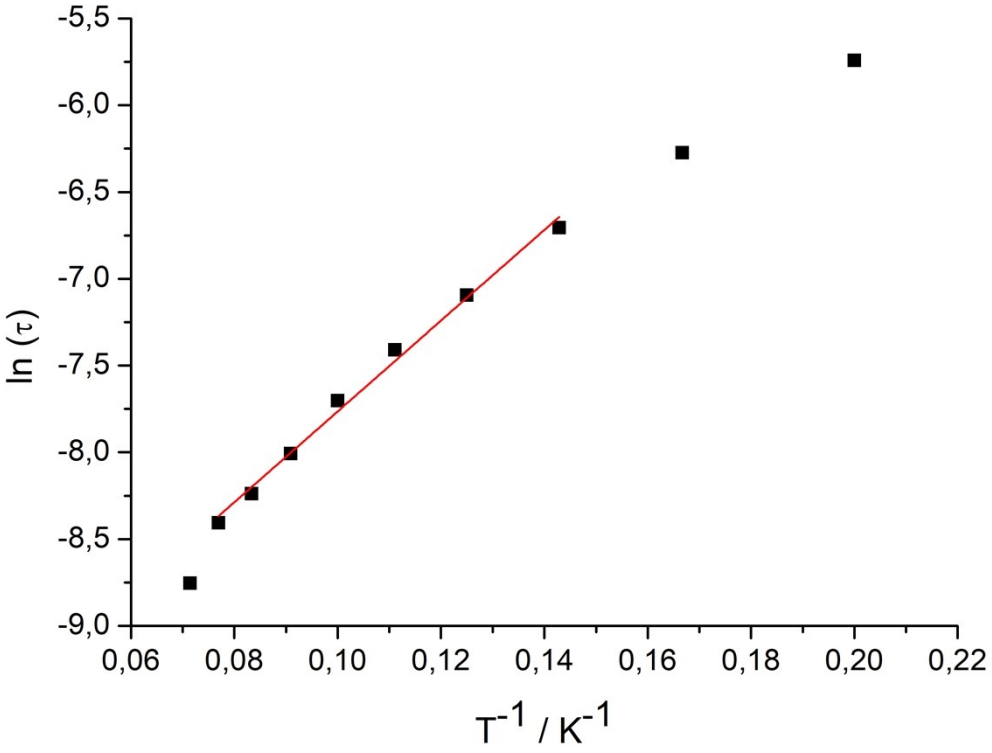

Figure S20. Fitting of the relaxation time for **5** using the Arrhenius law eq. 2.

The plot of ln(τ) vs 1/T shows a deviation from linearity, suggesting that a thermally activated Orbach relaxation is accompanied by other relaxation mechanisms (Raman and direct relaxation). On these grounds we tried to fit the entire range of temperature-dependent relaxation employing eq. 3, which enables the determination of the contributions from the other spin-lattice mechanisms. However, this invariably proved unsuccessful, and so the U_{eff} values determined above for the high-temperature regime (7-13K, Fig. S20) represent only an estimate and should be taken indicative rather than definitive.

$$\tau^{-1} = AT^{n} + \tau_0^{-1} \exp\left(-\frac{U_{eff}}{k_B T}\right) + CT^{m} \qquad (3)$$

Equation 3 includes three terms to account for the temperature-dependence of direct (AT^n), Orbach (second term), two-phonon Raman relaxation proesses (CT^m). The exponent *m*

describes the difference in the temperature dependence of Raman process for Kramers and non-Kramers ions (Kramers ions: m = 9; non-Kramers ions: m = 7).[5] The direct process often reveals a linear or quadratric dependence on the temperature, the exponents *n* being 1 or 2.[6]

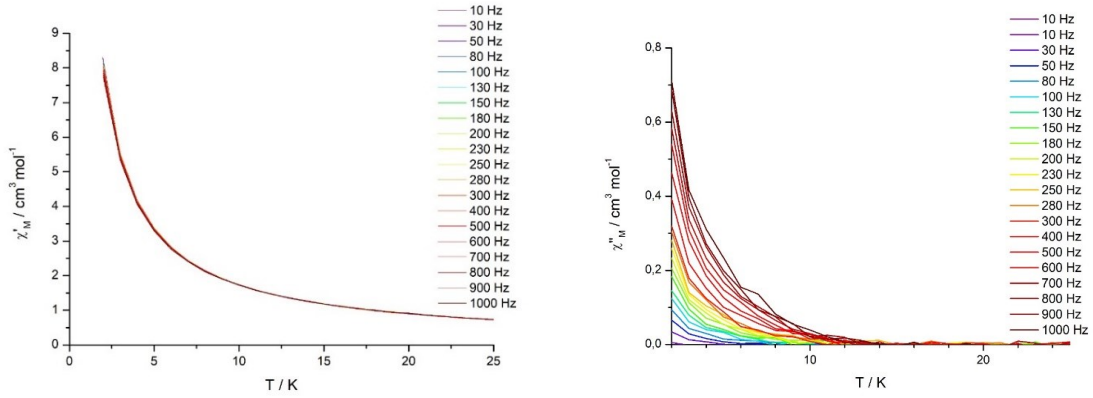

Figure S21. Temperature dependence of the in-phase (up) and out-of-phase (down) components of the ac magnetic susceptibility of $[Dy_2(L^2)_2]$ (**8**) in zero dc field.

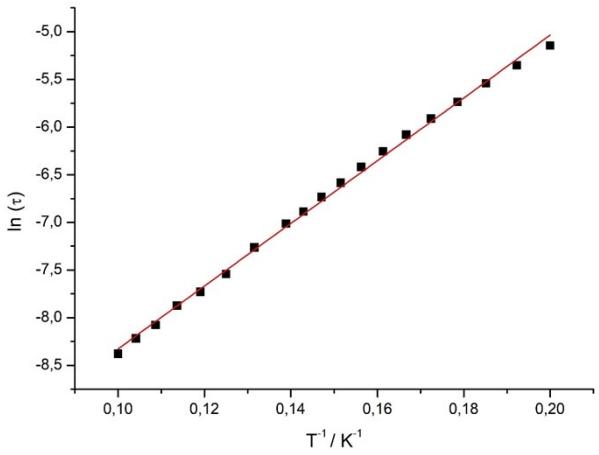

Figure S22 Fitting of the relaxation time for **8** using the Arrhenius law eq. 2.

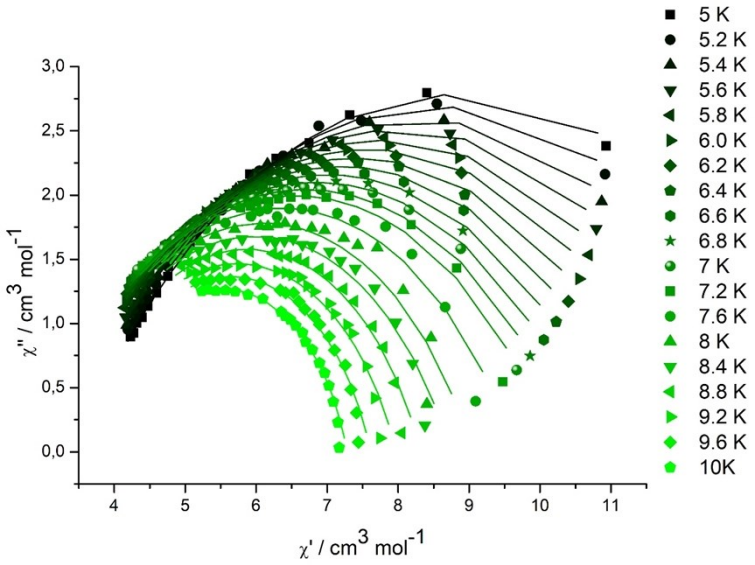

Figure S23. Plots of Cole-Cole fitting at selected temperatures (solid line for fitting) for compound **8**.

Table S2. Parameters resultant from fitting AC data of complex **8** (for 3 kOe).

T (K)	χ_S (cm^3/mol)	χ_T (cm^3/mol)	τ	α	Residual
5	3.46436	14.2117	0.00583	0.3915	0.11615
5.2	3.38160	13.7082	0.00473	0.3890	0.12000
5.4	3.28180	13.2603	0.00392	0.3912	0.12391
5.6	3.21674	12.8263	0.00323	0.3877	0.11749
5.8	3.12086	12.4665	0.00271	0.3905	0.13938
6	3.06852	12.1129	0.00229	0.3888	0.13370
6.2	3.00990	11.7561	0.00192	0.3867	0.14475
6.4	2.97187	11.3992	0.00163	0.3824	0.14086
6.6	2.93673	11.0724	0.00138	0.3790	0.14524
6.8	2.93824	10.7525	0.00119	0.3723	0.16243
7	2.93242	10.4638	0.00102	0.3674	0.15338
7.2	2.96237	10.1776	0.00090	0.3575	0.15628
7.6	3.06525	9.6371	0.00070	0.3338	0.17068
8	3.15645	9.0317	0.00053	0.3062	0.29176
8.4	3.22650	8.7302	0.00044	0.3029	0.15013
8.8	3.46065	8.3086	0.00038	0.2652	0.11763
9.2	3.51144	7.9667	0.00031	0.2589	0.94536
9.6	3.70218	7.6063	0.00027	0.2233	0.61292
10	3.80555	7.274	0.00023	0.1962	0.29441

References

[1] M. Llunell, D. Casanova, J. Cirera, P. Alemany, S. Alvarez, SHAPE version 2.1, University of Barcelona, Barcelona, 2013.

[2] S. Ullmann, P. Hahn, A. Mehnert, C. Laube, B. Abel, B. Kersting, *Dalt. Trans.* **2019**, *48*, 3893–3905.

[3] D. Reta, N. F. Chilton, *Phys. Chem. Chem. Phys.*, **2019**, *21*, 23567-23575.

[4] M. Grahl, J. Kotzler, I. Sessler, *J. Magn. Magn. Mater.* **1990**, *187*, 90-91.

[5] R. C. Mikkelson, H. J. Stapleton, *Phys. Rev.* **1965**, *140*, 1968-1982.

[6] K. R. Meihaus, S. G. Minasian, W. W. Lukens, Jr., S. A. Kozimor, D. K. Shuh, T. Tyliszczak, J. R. Long, *J. Am. Chem. Soc.* **2014**, *136*, 6056–6068.